ACS OMEGA

http://pubs.acs.org/journal/acsodf

Article

Coal Fly Ash Decorated with Graphene and Polyaniline Nanocomposites for Effective Adsorption of Hexavalent Chromium and Its Reuse for Photocatalysis

Emmanuel Christopher Umejuru, Eswaran Prabakaran, and Kriveshini Pillay*

Cite This: *ACS Omega* 2023, 8, 17523−17537

Read Online

ACCESS | Metrics & More | Article Recommendations

ABSTRACT: Coal fly ash was functionalized and modified with graphene oxide and polyaniline (CFA/GO/PANI nanocomposite) through hydrothermal synthesis, which was used for remediation of hexavalent chromium (Cr(VI)) ions. Batch adsorption experiments were carried out to investigate the effects of adsorbent dosage, pH, and contact time on the removal of Cr(VI). The ideal pH for this work was 2, and it was used for all other studies. The Cr(VI)-loaded spent adsorbent CFA/GO/PANI + Cr(VI) was reused as a photocatalyst for the degradation of bisphenol A (BPA). The CFA/GO/PANI nanocomposite removed Cr(VI) ions rapidly. The adsorption process was best described by pseudo-second-order kinetics and the Freundlich isotherm model. The CFA/GO/PANI nanocomposite demonstrated a high adsorption capacity of 124.72 mg/g for Cr(VI) removal. In addition, the Cr(VI)-loaded spent adsorbent played a significant role in the photocatalytic degradation of BPA with 86% degradation. The reuse of the Cr(VI)-loaded spent adsorbent as a photocatalyst presents a new solution for the reduction of secondary waste from the adsorption process.

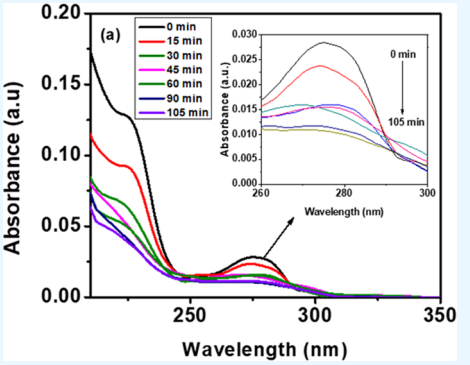

1. INTRODUCTION

The surge in industrial activities and population is a major driver of environmental pollution. The discharge of heavy metal ions and synthetic organic pollutants in large amounts into water bodies is of great concern. Among the various heavy metal ions of concern, hexavalent chromium (Cr(VI)) is eminent due to its high level of toxicity and availability in water.[1] The recommended concentration for Cr(VI) in drinking and surface water is 0.05 mg/L and 0.1 mg/L, respectively, based on the World Health Organization regulation.[2,3] Ingestion of Cr(VI) can cause cancer, tumors, and damage to DNA. Cr(VI) is discharged into water bodies from chemical industries, paint industries, dye production, tanning of leather, and several applications.[4−6] Synthetic organic pollutants are forms of contaminants known as emerging pollutants. Emerging pollutants refer to chemical substances without regulation, which have adverse effects that are yet to be clearly understood. The discharge of these pollutants into water bodies causes severe problems because of the challenges associated with their removal. Bisphenol A (BPA) is a famous emerging pollutant known to be an endocrine disruptor that is harmful to animals and humans.[7] These highlight the urgency for the development of economical and efficient methods for remediation of Cr(VI) and BPA from wastewater.

Different techniques such as membrane filtration, chemical precipitation, electrochemical remediation, bioremediation, ion exchange, and adsorption have been investigated for the remediation of Cr(VI) in wastewater.[8] Among these, attention and preference have been given to adsorption due to its relatively low cost of operation, ease of design, high removal efficiency, and reusability.[1,8] In addition, different adsorbents have been used in the adsorption of Cr(VI), which include biomaterials, clays, and agricultural and industrial wastes. However, low adsorption capacities have been reported for most of these materials due to the lack of robust surface functional groups, surface area, and stability.[9] Coal fly ash (CFA) is a cheap material produced as a waste product from thermal plants, which is known to be a resourceful material for the remediation of heavy metal ions in wastewater. Globally, more than 420 million tons of CFA is produced annually from thermal plants. Currently, due to a high demand for power, the release of CFA has increased. Nevertheless, less than 25% of the produced CFA is presently utilized.[10] Functionalization and surface modification of CFA are required to enhance its physical and chemical properties for better adsorption of heavy metal ions.

Graphene oxide (GO), which is synthesized from graphite, is a carbon-based material with excellent adsorption properties

Received: September 5, 2022
Accepted: December 6, 2022
Published: May 9, 2023

https://doi.org/10.1021/acsomega.2c05352
ACS Omega 2023, 8, 17523−17537

Scheme 1. Synthesis of the CFA/GO/PANI Nanocomposite

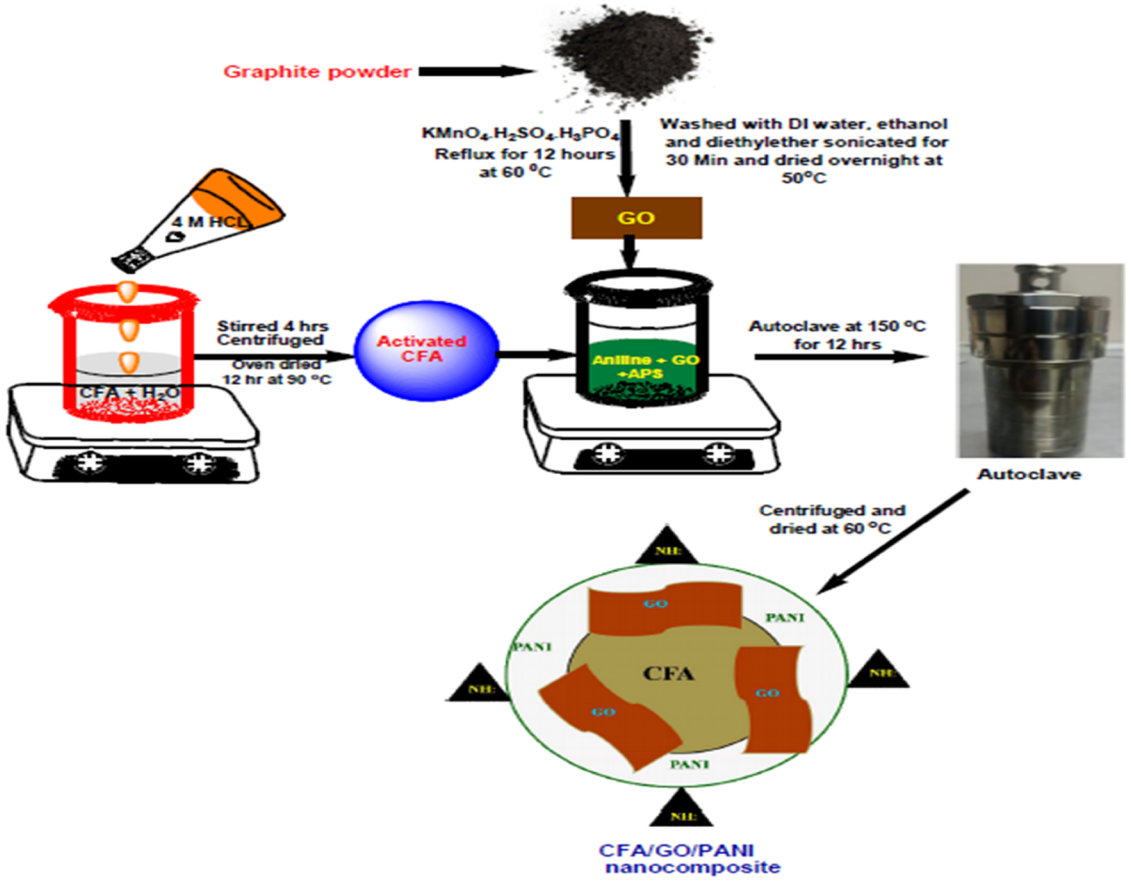

because of its rich functional groups (epoxy, hydroxyl, and carboxyl) and high surface area.[11] GO has been used to modify different materials for the adsorption of Cr(VI), and high adsorption capacities have been reported. For instance, Sahoo et al. fabricated a GO/$ZnOZnFe_2O_4$ nanocomposite for the adsorption of Cr(VI) and reported a removal of 109.89 mg/g.[12] Li et al. prepared a GO/Fe_3O_4 composite, which demonstrated a sorption capacity of 95.2 mg/g.[13] The incorporation of GO into suitable materials enhances its stability.[11]

Polymers are outstanding materials that have been used to modify other materials because of their efficiency, stability, conductivity, availability, affordability, and selectivity.[14] The necessity to minimize the concentration of heavy metal ions discharged into wastewater to levels within the recommended regulation and the possibility of their reuse have led to research on the application of selective polymer materials. Polyaniline (PANI) is among the conducting polymers with tremendous features such as high conductivity, ease of preparation, and suitable stability. PANI-based composites have been applied in the removal of heavy metal ions and catalytic processes for the degradation of organic pollutants.[15]

Photocatalysis is a notable advanced oxidation process widely used for degrading organic pollutants due to its great efficiency, ease of handling, simplicity, and awesome reproducibility. It is a cost-effective and environmentally friendly technique for the degradation of organic pollutants, whereby complete mineralization can be achieved.[16] Photodegradation is highly effective for the decomposition of organic pollutants (OPs) even at minute concentrations.[17] Additionally, its mechanism involves the reaction between vigorous oxidizing and reducing agents produced by visible or UV light on the catalyst and the organic pollutant.[18] During the treatment of industrial wastewater, heavy metals even in trace amounts are adsorbed on the edge of the catalyst. These adsorbed heavy metals have been found to be supportive in the photodegradation process, and Cr(VI) is among the common heavy metals present.[19,20] This is due to its photoelectrochemical property. Doping of materials with Cr can improve their interactions with light.[21]

An increasing number of spent adsorbents are generated after heavy metal adsorption. These spent adsorbents when discharged into the environment can cause secondary pollution. Discharge of the spent adsorbents into water bodies has become a global concern.[22] For example, high concentrations of the spent adsorbents have been found in the Sava river, which have caused different environmental problems.[23]

In this report, graphene oxide and polyaniline were incorporated into a coal fly ash (CFA/GO/PANI) nanocomposite for rapid removal of Cr(VI) from water and the Cr(VI)-loaded spent adsorbent (CFA/GO/PANI + Cr(VI)) was reused as a photocatalyst for the degradation of BPA.

2. MATERIALS AND METHODS

2.1. Materials. Aniline, sulfuric acid, graphite powder, potassium dichromate ($K_2Cr_2O_7$), phosphoric acid, bisphenol A, and ammonium persulfate were purchased from Sigma-Aldrich. Coal fly ash was obtained from a thermal power plant in South Africa.

2.2. Synthesis of the CFA/GO/PANI Nanocomposite. Deionized water (150 mL) and HCl (4M) were mixed with 100

https://doi.org/10.1021/acsomega.2c05352
ACS Omega 2023, 8, 17523−17537

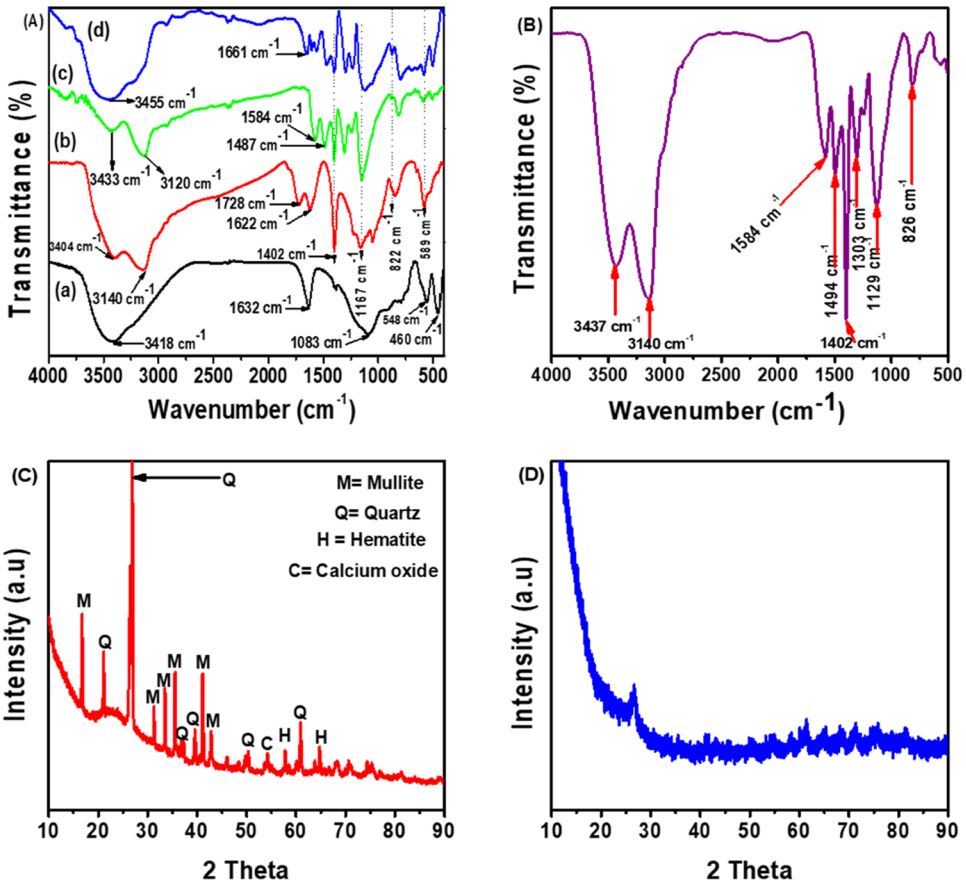

Figure 1. (A) FTIR spectra for (a) CFA, (b) synthesized GO, (c) synthesized PANI, and (d) CFA/GO/PANI nanocomposite and (B) CFA/GO/PANI + Cr(VI) and XRD patterns of (C) CFA and (D) CFA/GO/PANI nanocomposite.

g of CFA, which was magnetically stirred (4 h) to remove impurities and activate it. After the reaction, the solution was centrifuged with water and ethanol and dried in an oven (90 °C) for 12 h. The preparation of GO was achieved by modifying a technique stated elsewhere.[24] This was carried out through mixing 40 mL of H_3PO_4, 18 g of $KMnO_4$, 5 g of graphite, and 40 mL of H_2SO_4 and refluxing at 60 °C for 12 h. Then, H_2O_2 (30%) was used to quench the reaction mixture. The quenched reaction mixture was centrifuged using deionized water and ethanol for the removal of unwanted substances. A brownish-black precipitate of GO was obtained, sonicated (30 min), and kept in the oven at 50 °C for 12 h.

Finally, 4 g of activated CFA, aniline (3 mL), 3 g of GO added in 100 mL of HCL (1 M), and 9 g of ammonium persulfate (APS) dissolved in 20 mL of water were mixed and magnetically stirred for 24 h. At the end of the reaction, a dark-green precipitate was noticed due to polymerization, which was centrifuged with deionized water and ethanol to remove unwanted substances. The centrifuged mixture was added to 70 mL of deionized water and put in a 100 mL autoclave at 150 °C overnight. The nanocomposite was lastly obtained by centrifuging and drying in an oven at 60 °C. Scheme 1 shows the process of nanocomposite synthesis.

2.3. Characterization of the CFA/GO/PANI Nanocomposite. The prepared CFA/GO/PANI nanocomposite was characterized prior and after the experiment. The morphology was investigated with scanning electron microscopy (SEM, Tescan vega 3xmu), and the confirmation of particle size was achieved with transmission electron microscopy (TEM JEOL JEM-2100F). The investigation of band gap energy was carried out through diffuse reflectance spectroscopy using a Schimadzu UV-1208 model, Japan. The functional groups were identified using Fourier transform infrared (FTIR), KBr pellet press, using a Perkin-Elmer PE1600 FTIR spectrophotometer. The scanning ranged from 4000 to 400 cm^{-1}. A Malvern Zetasizer NanoZS 90 and X-ray powder diffraction (XRD) were used to measure the ζ-potential and confirm the crystallinity of CFA and amorphous nature of the prepared material. X-ray photoelectron spectroscopy (XPS) study was carried out with a Kratos Axis Ultra device, Kratos, U.K., monochromatic Al Kα radiation. The surface area was identified through Braunauer–Emmett–Teller (BET) analysis under nitrogen adsorption–desorption with a Micro-metrics, ASAP 2020 analyzer.

2.4. Batch Adsorption Studies. The batch experiments were carried out to explore the capability of the CFA/GO/PANI nanocomposite for Cr(VI) adsorption using a solution volume of 30 mL in plastic bottles (100 mL), which were put into a thermostatic incubator shaker at 200 rpm for 60 min, Separation Scientific, South Africa. A Cr(VI) stock solution of 1000 mg/L and serial dilution were used for different concentrations. The pH adjustment for Cr(VI) solutions was carried out by adding 0.1 M HCl and NaOH solutions before the addition of the adsorbents. Optimization of the conditions for adsorption was achieved by investigating the effect of different parameters (dosage, pH, Cr(VI) concentration, temperature, and contact time). Membrane filters (0.45 μm) were used to separate the CFA/GO/PANI nanocomposite from the solution after the reaction. The residual Cr(VI) concentration was analyzed by

https://doi.org/10.1021/acsomega.2c05352
ACS Omega 2023, 8, 17523−17537

measurement of absorbance (540 nm) with addition of a little amount of 1,5-diphenylcarbazide solution.[25]

The Cr(VI) percentage removal and adsorption capacity of the CFA/GO/PANI nanocomposite were estimated using eqs 1−3.

$$\text{removal}\ (\%) = \frac{(C_0 - C_e)}{C_0} \times 100 \quad (1)$$

$$q_t = \frac{(C_0 - C_t)V}{W} \quad (2)$$

$$q_e(\text{mg/g}) = \frac{(C_0 - C_e)V}{W} \quad (3)$$

where C_o, C_e, and C_t all in mg/L are the concentrations (initial, equilibrium, and final, respectively) of Cr(VI), q_e in mg/g refers to the amount of Cr(VI) adsorbed during the experiments, V refers to the volume of Cr(VI) in L, and W (g) refers to the total mass of the CFA/GO/PANI nanocomposite used.

2.5. Effect of Coexisting Ions. The study on the effect of coexisting ions was achieved by keeping the initial concentration of Cr(VI) constant at 100 mg/L, while varying that of lead (Pb^{2+}), nickel (Ni^{2+}), cadmium (Cd^{2+}), copper (Cu^{2+}), and manganese (Mn^{2+}) as 80 and 100 mg/L using a solution volume of 30 mL, optimized CFA/GO/PANI nanocomposite dosage (0.08 g), and pH 2.

2.6. Reuse of Cr(VI) Loaded on the CFA/GO/PANI Nanocomposite Spent Adsorbent. The spent adsorbent (CFA/GO/PANI + Cr(VI)) obtained after the batch experiment was reused as a photocatalyst for degradation of BPA. This was carried out by mixing 100 mg of the photocatalyst with 10 mg/L BPA in a 500 mL photoreactor, which was magnetically stirred in the dark for 30 min before photodegradation to achieve equilibrium. The visible light source used was a 250 HW lamp. The temperature was regulated all through the experiment by circulating cooled water via the photoreactor water inlet. Samples were taken at regular time intervals, and the solution was filtered using membrane filters (0.45 μM) to avoid further reaction. The BPA concentration left after degradation was determined using its maximum adsorption peak at 275 nm with an UV−visible spectrophotometer. All analyses were measured in triplicate.

The degradation efficiency of BPA was estimated using eq 4

$$\text{degradation}\ (\%) = \frac{C_o - C_t}{C_o} \times 100 \quad (4)$$

where C_o and C_t both in mg/L are the initial and final concentrations, respectively, after photodegradation.

3. RESULTS AND DISCUSSION

3.1. Characterization. *3.1.1. FTIR.* Functional groups play a vital role during the adsorption of heavy metal ions. FTIR investigation was conducted to identify the functional groups of the CFA/GO/PANI nanocomposite. The FTIR results for the CFA, synthesized GO, PANI, CFA/GO/PANI nanocomposite, and CFA/GO/PANI + Cr(VI) are presented in Figure 1A(a−d),B. The FTIR spectrum for CFA is shown in Figure 1A(a). The broad band at 3418 cm^{-1} was attributed to the stretching of OH. The peak at 1632 cm^{-1} was assigned to H−OH stretching.[26] The peak at 1083 cm^{-1} is associated with organic materials and the bending of Si−O.[27] The peaks at 548 and 460 cm^{-1} are assigned to minerals such as quartz and mullite, which were confirmed by XRD analysis.

The FTIR spectrum of GO is presented in Figure 1A(b) indicating the availability of various robust oxygen functional groups. The broad peak observed between 3404 and 3140 cm^{-1} is associated with the O−H stretching because of alcohol groups and also adsorbed molecules of water.[28] The peak at 1728 cm^{-1} is attributed to the stretching of C=O in the carboxylic acid group,[29] that at 1622 cm^{-1} is attributed to the C−O stretching vibration of COOH,[30] and that at 1402 cm^{-1} is assigned to the carboxyl vibration of C−OH.[29] The peaks at 1167, 1053, 848, and 590 cm^{-1} were due to the C−O stretching in C−O−C.[28,29] These confirm the successful formation of GO.

Figure 1A(c) shows the FTIR spectrum of the synthesized PANI. The peaks at 1584 and 1487 cm^{-1} are due to the C=C vibration of benzenoid and quinoid rings.[31] The peaks at 1399 and 1302 cm^{-1} are attributed to the stretching of C−N, whereas those at 1152 and 822 cm^{-1} are assigned to the $-NH^{+}=$ vibration and C−H twisting of the benzene ring, respectively.[32] The presence of these peaks confirmed the successful preparation of PANI.

For the FTIR spectrum of the CFA/GO/PANI nanocomposite (Figure 1A(d)), there was a slight shift in the peak position, and the peak intensities were reduced. Furthermore, new peaks appeared at 1661 and 1573 cm^{-1} corresponding to the N−H vibration of the benzene ring[33] and C−C skeleton vibration on the graphene oxide surface,[34] that at 1497 cm^{-1} corresponds to the aromatic skeletal vibration of the (C=C) bond,[35] and those at 1304 cm^{-1} (C−N) and 1583 cm^{-1} are associated with the availability of silica in CFA onto the CFA/GO/PANI nanocomposite. Moreover, the peaks at 1728 and 1622 cm^{-1} disappeared due to the strong interactions that occurred between GO, PANI, and the various metal oxides in CFA.[36] This contributed significantly to the adsorption observed. Disappearance and formation of new peaks are usually expected after hybridization.[34]

FTIR analysis was conducted after adsorption to understand the changes in vibration frequencies and to investigate the interactions between Cr(VI) and the CFA/GO/PANI nanocomposite as displayed in Figure 1B. The FTIR spectra after adsorption showed major changes in terms of peak positions and intensities. The O−H peaks shifted from 3455 cm^{-1} to intense peaks at 3437 and 3140 cm^{-1}. The C−C skeleton vibration at 1573 cm^{-1} shifted to 1584 cm^{-1}, and the (C=C) bond at 1497 cm^{-1} shifted to 1494 cm^{-1}. The peaks at 1400 and 1304 cm^{-1} shifted slightly to more intense peaks at 1402 and 1303 cm^{-1}. The peak at 1583 cm^{-1} is due to the presence of silica in the CFA/GO/PANI nanocomposite, which disappeared after adsorption of Cr(VI). The C−O stretching vibration in C−O−C at 820 cm^{-1} shifted to 826 cm^{-1}, while that of 586 cm^{-1} disappeared after the adsorption of Cr(VI). These various functional groups were actively involved in the successful adsorption of Cr(VI) and those that disappeared such as N−H, C−N, and the peak for silica were due to their coordination with Cr(VI). A new peak appeared after adsorption at 1129 cm^{-1}, and this was associated with the stretching of Cr=O.[35] These confirm that the interaction between the functional groups on the CFA/GO/PANI nanocomposite and Cr(VI) is complexation.[37]

3.1.2. X-ray Diffraction Spectroscopy (XRD). XRD analysis helps to reveal the crystallinity or amorphous nature of materials, which are beneficial in the adsorption process. Figure 1C,D presents the XRD spectra of the CFA and CFA/GO/PANI

https://doi.org/10.1021/acsomega.2c05352
ACS Omega 2023, 8, 17523−17537

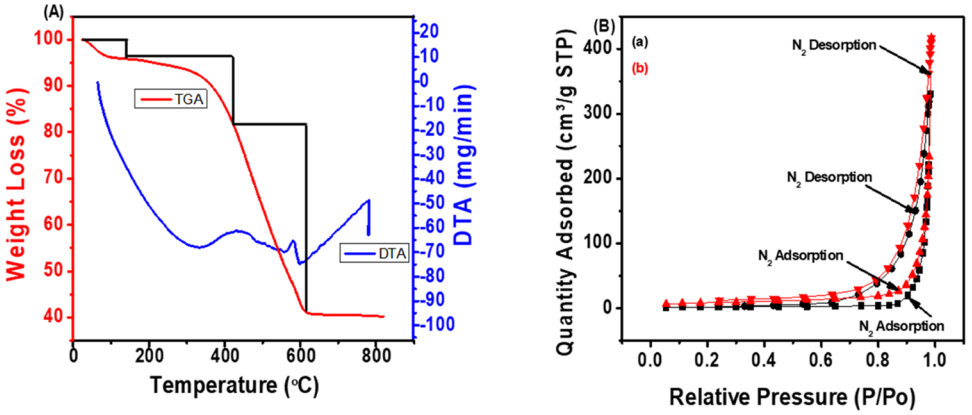

Figure 2. (A) Thermogravimetric analysis (TGA) and differential thermal analysis (DTA) of the CFA/GO/PANI nanocomposite. (B) Nitrogen adsorption−desorption isothermal curves of (a) CFA and (b) CFA/GO/PANI nanocomposite.

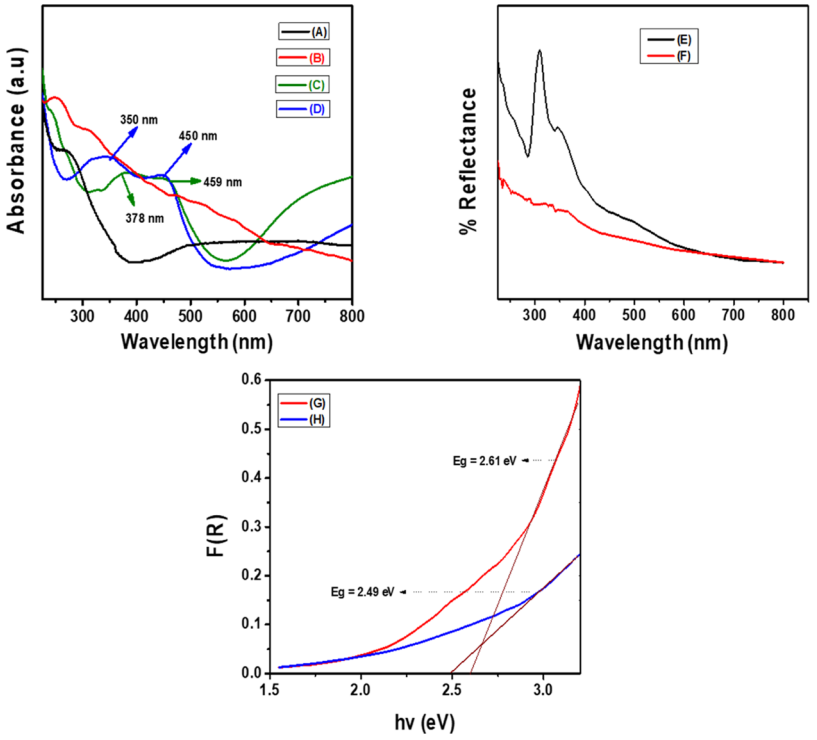

Figure 3. UV spectra for (A) CFA, (B) synthesized GO, (C) synthesized PANI, and (D) CFA/GO/PANI nanocomposite, energy gap investigation for (E) CFA/GO/PANI nanocomposite and (F) CFA/GO/PANI + Cr(VI), and Tauc plot for (G) CFA/GO/PANI nanocomposite and (H) CFA/GO/PANI + Cr(VI).

nanocomposite. It is obvious from Figure 1C that CFA consists of crystalline phases such as mullite (M, $Al_6Si_2O_{13}$), and quartz (Q, SiO_2) with lower amounts of hematite (H, Fe_2O_3) and lime or calcium oxide (CaO), which correlate with the FTIR spectrum of CFA. Figure 1D reveals that the XRD spectrum of the CFA/GO/PANI nanocomposite showed a decrease in peak intensity for the peaks of M, Q, and H, which is indicative of the amorphous nature due to the interaction of CFA with GO and PANI.[38,39] This confirms the successful incorporation of GO and PANI into CFA, which were highly effective in the modification and functionalization of CFA for the efficient adsorption of Cr(VI).

3.1.3. Thermal Analysis. The pattern for thermal degradation of the CFA/GO/PANI nanocomposite showed two weight losses as displayed in Figure 2A. The initial weight loss ranges from 29 to 140 °C corresponding to 4% due to the loss of water molecules adsorbed on the CFA/GO/PANI nanocomposite. The second weight loss observed was 14% from 140 to 421 °C. The weight loss (40.68%) occurred from 421 to 600 °C. These are associated with the decomposition of various oxygen groups, which include OH, COOH, and CO.[40] The material becomes stable above 600 °C due to the interaction between CFA, GO, and PANI, indicating the stability of the synthesized CFA/GO/PANI nanocomposite.[41]

3.1.4. BET. Specific surface area plays a vital role during the adsorption of heavy metal ions. BET analysis was used to investigate the surface area of CFA and the CFA/GO/PANI nanocomposite. Figure 2B(a,b) shows that the nitrogen adsorption−desorption isotherm curves for CFA and the CFA/GO/PANI nanocomposite closely match the type III adsorption isotherm. Both the CFA and CFA/GO/PANI nanocomposite were made up of mesoporous and microporous

https://doi.org/10.1021/acsomega.2c05352
ACS Omega 2023, 8, 17523−17537

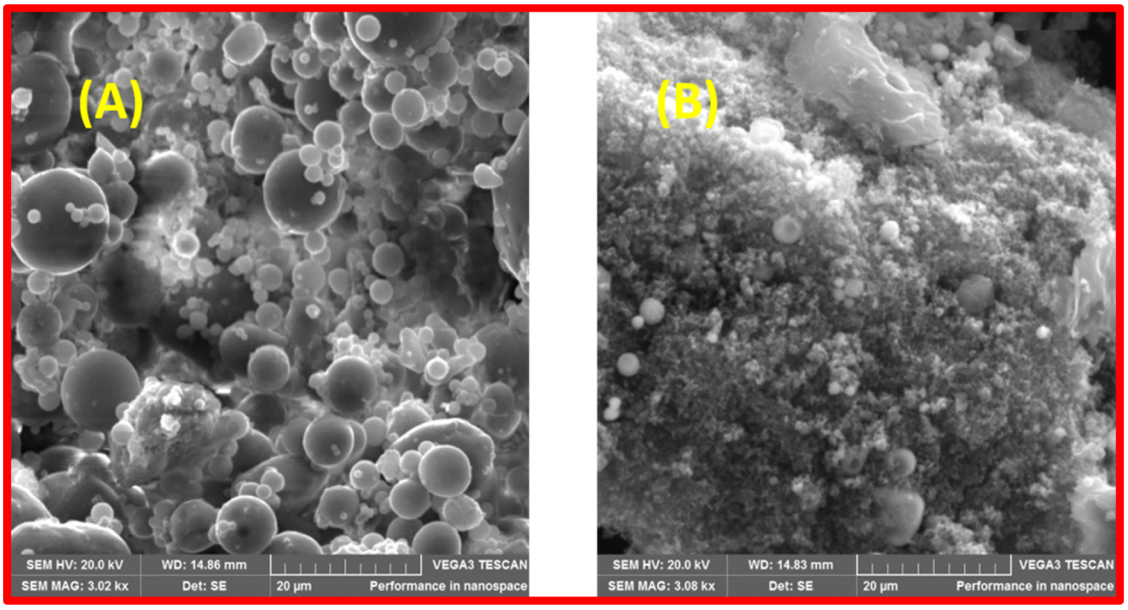

Figure 4. SEM images of (A) CFA and (B) CFA/GO/PANI nanocomposite.

structures.[42] The estimated values for the surface area of CFA and the CFA/GO/PANI nanocomposite were 5.5699 and 30.2580 m^2/g, respectively. The surface area of the CFA/GO/PANI nanocomposite increased 6-fold when compared to that of CFA. The increased specific surface area of the CFA/GO/PANI nanocomposite provided active sites, which contributed significantly to the effective adsorption of Cr(VI).

3.1.5. UV−vis Spectroscopy. Further investigation was carried out using UV−vis spectroscopy to confirm the formation of PANI and its interaction in the CFA/GO/PANI nanocomposite aside from that observed in the FTIR analysis. Figure 3A−D presents the spectra of CFA, GO, PANI, and the CFA/GO/PANI nanocomposite. The as-prepared PANI showed peaks at 378 nm and 459 nm. These peaks are associated with the $\pi \rightarrow \pi^*$ transition band of the benzenoid ring and polaronic peak, revealing polymer protonation.[31,43] The peaks shifted slightly for the CFA/GO/PANI nanocomposite due to the interaction of PANI with CFA and GO. Both CFA and GO did not record any absorption peaks in the (300−800) nm range.

The energy gaps of the CFA/GO/PANI nanocomposite and CFA/GO/PANI + Cr(VI) were investigated using UV−visible diffuse reflection spectra presented in Figure 3E,F. The determined energy gaps for the CFA/GO/PANI nanocomposite and CFA/GO/PANI + Cr(VI) using Tauc plots are 2.62 and 2.49 eV, as shown in Figure 3G,H. These revealed that the energy gap of the CFA/GO/PANI nanocomposite reduced after Cr(VI) adsorption, which contributed to the effective degradation of BPA.

3.1.6. Morphology. The morphologies of CFA and the CFA/GO/PANI nanocomposite were investigated by SEM as presented in Figure 4A,B. The SEM image of CFA reveals spherical structures as shown in Figure 4A. The SEM image for the CFA/GO/PANI nanocomposite (Figure 4B) shows that the modification of CFA with GO and PANI formed sphere-, sheet-, and fiber-like structures, which were significant for the high adsorption of Cr(VI) due to the provision of more sites.[44]

3.1.7. TEM. The structure of nanomaterials plays a major role during heavy metal ion adsorption by providing more adsorption sites. The characteristics of the CFA/GO/PANI nanocomposite were further investigated using TEM to determine its structure and size. The interconnected layer structure of nanosheets of CFA, GO, and PANI with enormous pores and channels can be noticed at a low magnification (200 nm) as indicated in Figure 5A. Large sizes of connection sheets

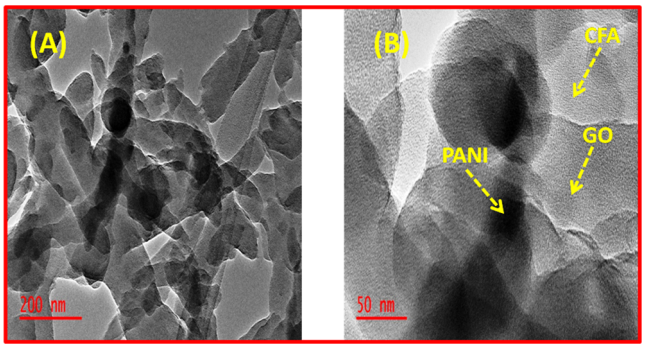

Figure 5. TEM images at different magnifications of (A) 200 nm (B) 50 nm.

of CFA, GO, and PANI were revealed at a higher magnification of 50 nm as presented in Figure 5B. These interconnected layers and porous structures provided active sites for effective adsorption of Cr(VI).

3.1.8. XPS. Figure 6A,B displays the XPS spectra of the CFA/GO/PANI nanocomposite (A) prior and (B) after adsorption. The survey scan of the CFA/GO/PANI nanocomposite (Figure 6A(a)) presents energy bands at 171.88, 201.17, 286.24, 402.35, and 530.47 eV, assigned to Al, Si, C 1s, N 1s, and O 1s, respectively. The XPS spectrum of O 1s revealed a peak at 531.43 eV as presented in Figure 6A(b). The XPS spectrum of C 1s presents a peak at 284.60 eV as shown in Figure 6A(c). The survey scan after adsorption of Cr(VI) presents a new peak assigned to Cr 2p as indicated in Figure 6B(a). The XPS spectrum of O 1s after adsorption shifted from 531.43 to 531.18 eV, which moved to a lower binding energy of 0.25 eV as displayed in Figure 6B(b). The XPS spectrum of C 1s after adsorption (Figure 6B(c)) shifted slightly to 284.67 eV,

https://doi.org/10.1021/acsomega.2c05352
ACS Omega 2023, 8, 17523−17537

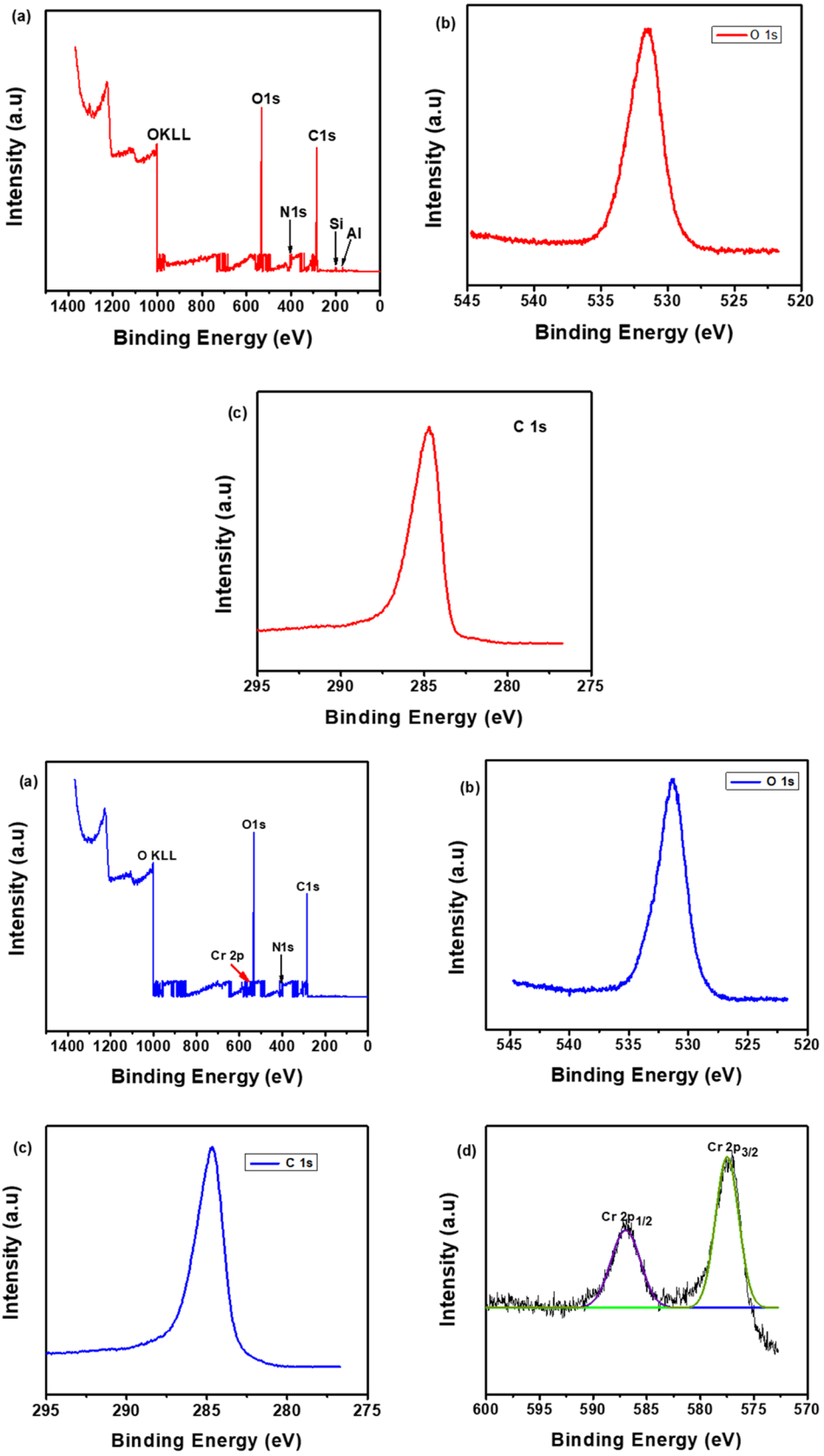

Figure 6. (A) XPS before adsorption, (a) survey scan for the CFA/GO/PANI nanocomposite, (b) O 1s, and (b) C 1s. (B) XPS after adsorption, (a) survey scan for CFA/GO/PANI + Cr(VI), (b) O 1s, (c) C 1s, and (d) Cr 2p.

indicating that there was no major change in the carbon chain.[45] Figure 6B(d) shows the deconvolution peak of Cr 2p with peaks at 577.37 (Cr $2p_{3/2}$) and 586.92 eV (Cr $2p_{1/2}$) associated with Cr(III).[1,45] These results confirm the efficiency

https://doi.org/10.1021/acsomega.2c05352
ACS Omega 2023, 8, 17523−17537

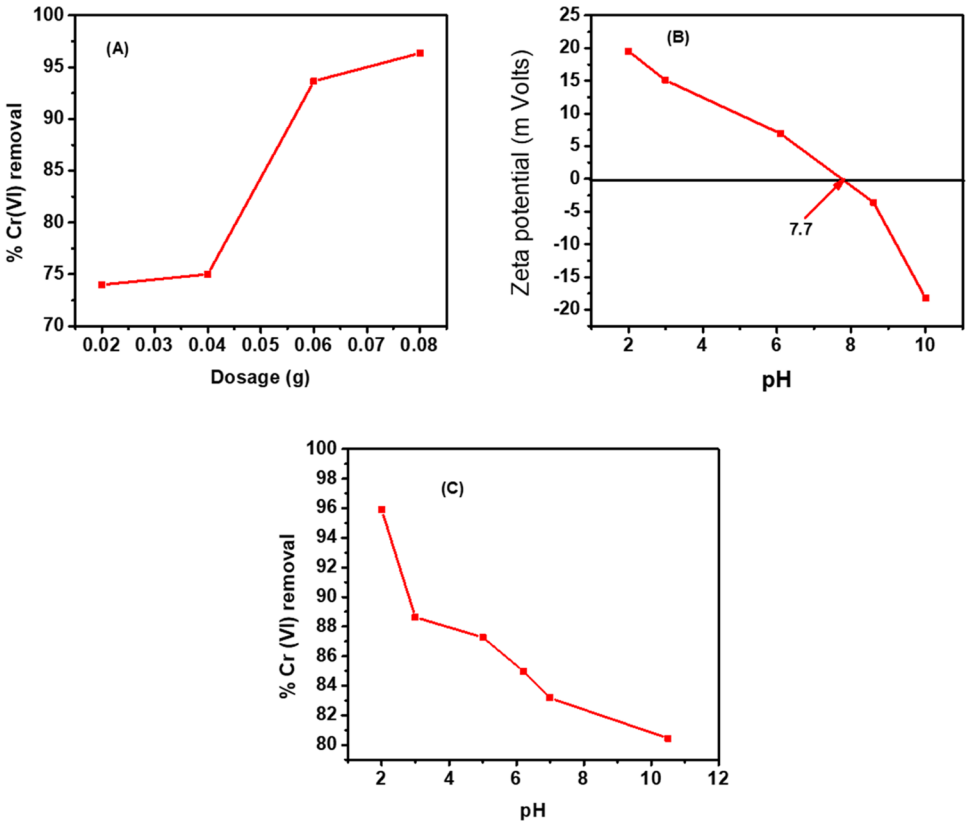

Figure 7. Effect of various parameters, (A) dosage, (B) ζ-potential, and (C) pH.

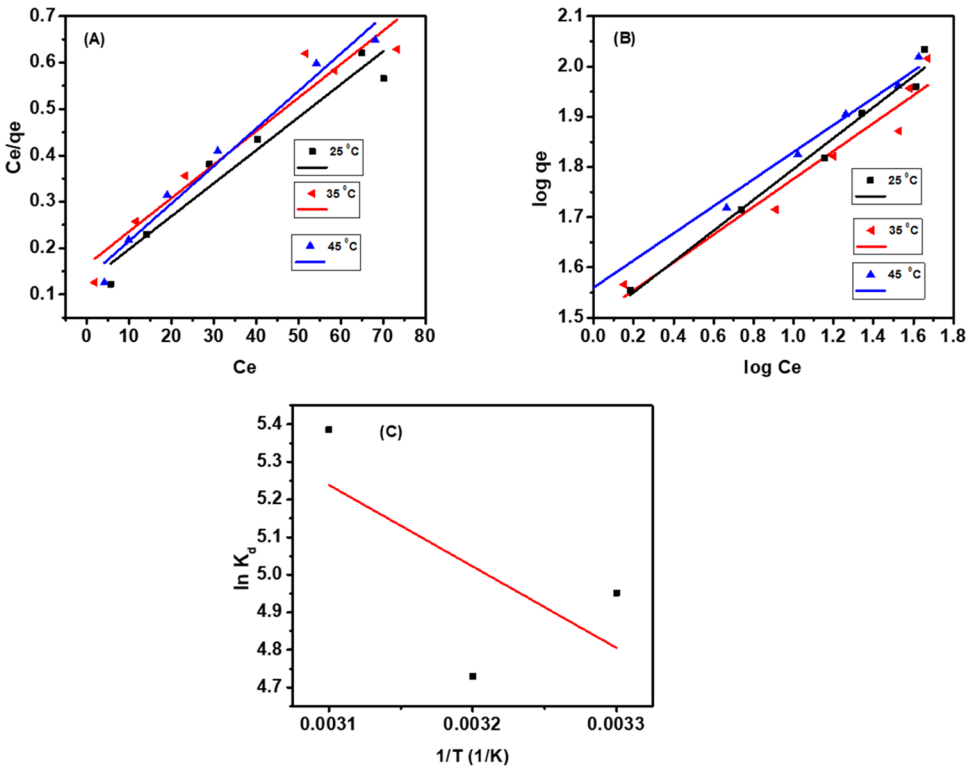

Figure 8. (A) Langmuir, (B) Freundlich, and (C) thermodynamic plot.

of the CFA/GO/PANI nanocomposite in the adsorption and reduction of Cr(VI).

3.2. Batch Adsorption Study. *3.2.1. Effect of the Adsorbent Dosage on Cr(VI) Adsorption onto the CFA/GO/PANI Nanocomposite.* The study on the dosage effect was achieved by varying the CFA/GO/PANI nanocomposite dose (0.02−0.08 g) using 30 mL of 100 mg/L Cr(VI) solution as shown in Figure 7A. It was revealed that an increase in the

https://doi.org/10.1021/acsomega.2c05352
ACS Omega 2023, 8, 17523−17537

adsorbent dosage led to an increase in the percentage removal of up to 96.41%; this is because of the increase in the number of active sites.[46] Therefore, 0.08 g was used throughout the experiments.

3.2.2. ζ-Potential Analysis. The point of zero charge of nanomaterials helps in the explanation of the adsorption mechanism and elucidation of the pH effect on heavy metal ion removal. The point of zero charge of the CFA/GO/PANI nanocomposite was pH 7.7 as displayed in Figure 7B. Below pH 7.7, the surface of the CFA/GO/PANI nanocomposite becomes positively charged, which is due to the protonation of functional groups, and favors the adsorption of Cr(VI) by electrostatic interactions. Nevertheless, above pH 7.7, deprotonation of the surface functional groups of the CFA/GO/PANI nanocomposite takes place and the surface becomes negatively charged, thus leading to a decline in the removal of Cr(VI) due to electrostatic repulsion and competition between CrO_4^{2-} and OH^-.[1,47,48]

3.2.3. Effect of pH on Cr(VI) Adsorption onto the CFA/GO/PANI Nanocomposite. The adsorption process can be significantly affected by the solution pH. The investigation of the pH effect on the adsorption of Cr(VI) onto the CFA/GO/PANI nanocomposite was achieved by varying the pH (2 to 10.5) as presented in Figure 7C. It can be noticed from the result that there was a drastic decrease in the percentage removal of Cr(VI) ions from 96% at pH 2 to 80% at pH 10.5. This shows that pH has a strong effect on Cr(VI) adsorption onto the CFA/GO/PANI nanocomposite. At various pH values, Cr(VI) exists in different states (CrO_4^{2-}, $Cr_2O_7^{2-}$, $HCrO_4^-$, and H_2CrO_4), where $HCrO_4^-$ dominates at lower pH 2. The higher percentage removal at pH 2 is because of the strong electrostatic interaction between $HCrO_4^-$ and the positively charged surface particles of the CFA/GO/PANI nanocomposite. The reduction of percentage removal at higher pH is because of the competition between OH^- and CrO_4^{2-} and electrostatic repulsion between Cr(VI) and the negatively charged surface particles of the CFA/GO/PANI nanocomposite.[48]

3.2.4. Adsorption Isotherms. The determination of the adsorption capacity of the CFA/GO/PANI nanocomposite and thermodynamics of its Cr(VI) removal was carried out by investigating the effect of temperature. This was evaluated at constant temperatures (25, 35, and 45 °C) and pH 2 using 30 mL of 100−350 mg/L initial Cr(VI) ion concentration and 0.08 g of the CFA/GO/PANI nanocomposite for 80 min. Figure 8A,B presents the linear plots of Langmuir and Freundlich isotherms, respectively. Although both the Langmuir and Freundlich isotherms show a good fit, the Freundlich isotherm still presents the best fit as shown in Table 1. The linear forms of Langmuir and Freundlich isotherms are shown in eqs 5 and 6, respectively.

Langmuir equation:

$$\frac{C_e}{q_e} = \frac{1}{bq_m} - \frac{C_e}{q_m} \tag{5}$$

Freundlich equation:

$$\log q_e = \log k_f + \frac{1}{n} \log C_e \tag{6}$$

where C_e (mg/L) and q_e (mg/g) refer to the Cr(VI) ion solution concentration and quantity of Cr(VI) ions adsorbed at the equilibrium state, respectively; q_m and b are the Langmuir constant associated with the maximum adsorption capacity and binding energy, respectively; and K_f and n are the Freundlich constant and adsorption intensity, respectively. The dimensionless separation factor R_L is shown in eq 7, which reveals adsorption feasibility.

Table 1. Isotherms for Cr(VI) Adsorption onto the CFA/GO/PANI Nanocomposite

	temperature (°C)		
parameters	25	35	45
	Langmuir		
q_m(mg/g)	124.72	106.04	122.5
R^2	0.9365	0.9209	0.9708
b(L/mg)	0.0612	0.0953	0.1815
R_L	0.0925	0.0620	0.0330
	Freundlich		
k_f(mg/g)	19.57	29.71	36.75
n	2.53	3.81	3.42
R^2	0.97744	0.92709	0.98832

$$R_L = \frac{1}{1 + bC_o} \tag{7}$$

where C_o in mg/L is the initial concentration and b (L/mg) refers to the Langmuir constant. The R_L ranging between 0 and 1 suggests a favorable adsorption system. In this study, the R_L results obtained (Table 1) were between 0 and 1, revealing that the adsorption process is favorable. The CFA/GO/PANI nanocomposite was compared with other adsorbents applied in the removal of Cr(VI) as indicated in Table 2.

Table 2. Comparison of Adsorption Capacity of the CFA/GO/PANI Nanocomposite with Different Adsorbents Applied for the Removal of Cr(VI) from Aqueous Solution

s.no	adsorbents	adsorption capacity (mg/g)	isotherms	references
1	GO/ZnOZnFe$_2$O$_4$ nanocomposite	109.89	Langmuir	12
2	GO/Fe$_3$O$_4$ composite	95.2	Langmuir	13
3	polyaniline/zeolite	5.97	Freundlich	38
4	PANI/EC	38.76	Langmuir	47
5	clay−rhizobium biosorbent	22.22	Langmuir	49
6	CFA/GO/PANI nanocomposite	**124.72**	**Langmuir**	**this study**

3.2.5. Thermodynamics. The adsorption mechanism of Cr(VI) ions onto the CFA/GO/PANI nanocomposite was further investigated from the adsorption isotherm and thermodynamic parameters of Gibbs free energy ($\Delta G°$), enthalpy ($\Delta H°$), and entropy ($\Delta S°$) using eqs 8 and 9

$$\Delta G = -RT \ln K_d = -RT \ln\left(m\frac{q_e}{C_e}\right) \tag{8}$$

$$\ln K_d = \ln\left(m\frac{q_e}{C_e}\right) = \frac{\Delta S°}{R} - \frac{\Delta H°}{RT} \tag{9}$$

where K_d is the thermodynamic equilibrium constant, m in g/L is the adsorbent dose, mq_e/C_e is the adsorption affinity, R (0.008314 kJ/mol/K) is the gas constant, and T is the temperature (kelvin). The values of $\Delta S°$ and $\Delta H°$ were estimated from the plot (slope and intercept) of $\ln(mq_e/C_e)$ presented in Figure 8C. Table 3 shows the results obtained for

https://doi.org/10.1021/acsomega.2c05352
ACS Omega 2023, 8, 17523−17537

Table 3. Thermodynamics for Cr^{+6} Adsorption onto the CFA/GO/PANI Nanocomposite

temperature (K)	$\Delta H°$ (kJ/mol)	$\Delta S°$ (kJ/mol)	$\Delta G°$ (kJ/mol)
298	18.02	0.0994	−11.60
308			−12.59
318			−13.59

the thermodynamic parameters. The positive value of $\Delta H°$ reveals the endothermic nature of the adsorption process. Contrarily, the negative increase in the value for $\Delta G°$ shows the feasibility and a spontaneous reaction, confirming that temperature favored the adsorption process. This can be attributed to a higher adsorption driving force due to the surged mobility in the solution. A positive value obtained for $\Delta S°$ indicates the heightened randomness in the process of adsorption.[1]

3.2.6. Time Effect on Cr(VI) Adsorption onto the CFA/GO/PANI Nanocomposite and Adsorption Kinetics. Adsorption kinetics can be used to investigate the controlling step of the adsorption rate, thereby providing information for modeling adsorption treatment techniques.[50] The contact time effect on Cr(VI) adsorption onto the CFA/GO/PANI nanocomposite was investigated in the temperature range of 25, 35, and 45 °C and the time interval of 10−80 min using an initial Cr(VI) concentration of 100 mg/L. The equilibrium times for all temperatures were estimated at 80 min as shown in Figure 9A. The linear forms of the pseudo-first order and pseudo-second order were used to evaluate the adsorption data (eqs 10 and 11).

Pseudo-first-order linear form is

$$\log(q_e - q_t) = \log q_e - \frac{k_1}{2.303}t \quad (10)$$

pseudo-second-order linear form is

$$\frac{t}{q_t} = \frac{1}{k_2 q_e^2} + \frac{1}{q_e}t \quad (11)$$

where q_e and q_t, both in mg/g, refer to the quantity of Cr(VI) ions adsorbed at equilibrium and time t, respectively, and k_1 (min^{-1}) and k_2 (g/min/mg) represent the pseudo-first-order and pseudo-second-order rate constants, respectively. The estimation of parameters was obtained from the linear plot of $\log(q_e - q_t)$ against t for the pseudo-first-order model and t/q_t against t for the pseudo-second-order model.

Figure 9B,C shows the linear plots of the pseudo-first-order and pseudo-second-order models. The estimated values for kinetic parameters are shown in Table 4. The obtained results

Table 4. Kinetics Models and Parameters for the Adsorption of Cr^{6+} onto the CFA/GO/PANI Nanocomposite

	temperature (°C)		
parameters	25	35	45
	Pseudo-First Order		
R^2	0.9029	0.89512	0.9616
K_1 (min^{-1})	0.0457	0.0559	0.0642
q_e(mg/g)	6.2991	7.8957	10.1365
	Pseudo-Second Order		
q_e(mg/g)	2.0197	21.3447	18.5391
R^2	0.9998	0.99985	0.99989
k_2(g/mg/min)	9.1158	0.0828	0.1111
	Intraparticle Diffusion Model		
k_i(mg/g/$min^{0.5}$)	0.7215	0.6841	0.8851
C(mg/g)	30.52	31.37	30.17
R^2	0.825	0.90604	0.84574

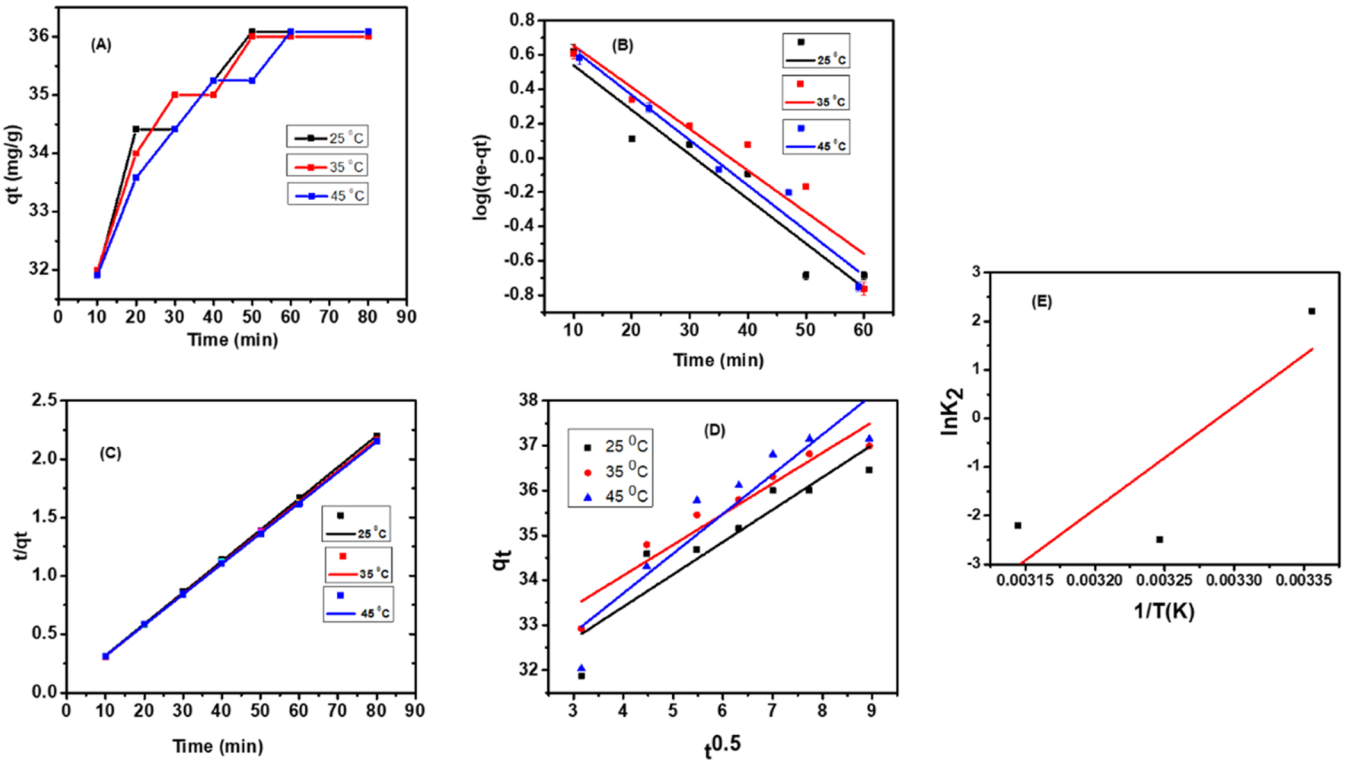

Figure 9. (A) Effect of contact time at 25, 35, and 45 °C, (B) pseudo-first-order, (C) pseudo-second-order, (D) intraparticle diffusion, and (E) activation energy.

https://doi.org/10.1021/acsomega.2c05352
ACS Omega 2023, 8, 17523−17537

for R^2 from the pseudo-second-order model are closer to unity compared to those of the pseudo-first order as indicated in Table 4. Therefore, the adsorption of Cr(VI) ions onto the CFA/GO/PANI nanocomposite followed the pseudo-second-order model.

The investigation of the rate-controlling step was estimated using the Webber−Morris intraparticle diffusion model presented in eq 12.

$$q_t = K_i t^{0.5} + C \tag{12}$$

where K_i (mg/g/min$^{0.5}$) is the intraparticle rate constant and C (mg/g) refers to the intercept representing the thickness of the boundary layer. The plots of q_t against $t^{0.5}$ for different temperatures and estimated values for intraparticle parameters are presented in Figure 9D and Table 4. Intraparticle diffusion is the sole process that controls the adsorption process if the plot passes through the origin. It can be observed that the plots did not go through the origin. Thus, the adsorption process was not totally controlled by intraparticle diffusion.[1]

Furthermore, the activation energy (E_a) was investigated using the Arrhenius equation as indicated in eq 13. The rate constant K_2 (g/mg/min) was obtained from the pseudo-second-order model at various temperatures.

$$\ln K_2 = \ln A - \frac{E_a}{RT} \tag{13}$$

where A (g/mg/min) is the frequency factor and E_a (kJ/mol) is the activation energy of adsorption. E_a was estimated from the plot of $\ln K_2$ against $1/T$ as presented in Figure 9E. The estimated value for activation energy is 176 kJ/mol, which reveals a chemisorption.[51,52]

3.2.7. Effect of the Coexisting Ions. Cr(VI) can coexist with other heavy metal ions that may compete with it during adsorption in real wastewater samples. Thus, investigation was carried out on the effect of different coexisting ions on the adsorption of Cr(VI) by the CFA/GO/PANI nanocomposite using lead (Pb^{2+}), nickel (Ni^{2+}), cadmium (Cd^{2+}), copper (Cu^{2+}), and manganese (Mn^{2+}). The initial concentration of Cr(VI) was kept constant at 100 mg/L, whereas those of the coexisting ions were varied between 80 and 100 mg/L at optimized dosage and pH 2. Figure 10 displays the result for the coexisting ions. It can be noticed that Pb^{2+} showed no serious effect on Cr(VI) adsorption at both concentrations of (80 and 100) mg/L, while the presence of others exerted significant competing effects. This can be attributed to the charge radius (Z/r, Å) of these ions.[53] Since the surface charge of the CFA/GO/PANI nanocomposite becomes positive below pH 7.7, it could attract chromium anions, while repelling the coexisting cations. Nevertheless, the cations could also mix with chromium anions, which greatly affected the removal efficiency.[54]

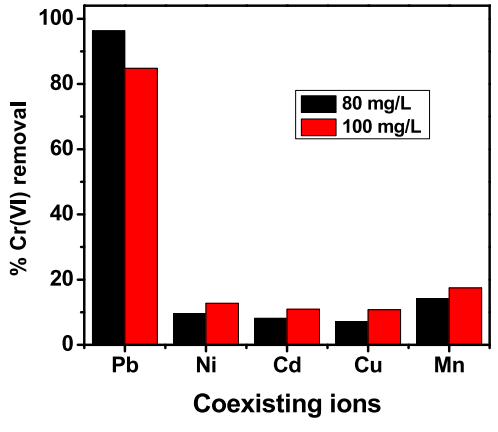

Figure 10. Effect of coexisting ions.

3.2.8. Mechanism of Cr(VI) Adsorption onto the CFA/GO/PANI Nanocomposite. The adsorption mechanism can be understood from the effect of pH and FTIR and XPS investigation prior and after adsorption as explained in detail above. The effect of pH revealed that there are electrostatic interactions between Cr(VI) and the CFA/GO/PANI nanocomposite. The changes in FTIR peaks after adsorption revealed the successful adsorption of Cr(VI) onto the CFA/GO/PANI nanocomposite. Further analysis using XPS confirms Cr 2p with peaks at 577.37 (Cr $2p_{3/2}$) and 586.92 eV (Cr $2p_{1/2}$) after adsorption. From the above-mentioned results, it can be summarized that the mechanism of Cr(VI) adsorption onto the CFA/GO/PANI nanocomposite is electrostatic interaction because of the protonation of the robust oxygen-containing functional groups on the CFA/GO/PANI nanocomposite[55] shown in Scheme 2. There is also evidence of reduction of Cr(VI) to Cr(III) from the XPS results.

3.3. Investigation on the Reusability of CFA/GO/PANI + Cr(VI) for Photocatalytic Degradation of BPA. The newly prepared nanocomposite, CFA/GO/PANI, was demonstrated to be highly effective for the removal of toxic heavy metals such as Cr(VI) from water. The spent adsorbent (CFA/GO/PANI + Cr(VI)), generated after the removal of Cr(VI) from water, was reused as a photocatalyst for the degradation of BPA. This was carried out using 10 ppm BPA in a 500 mL solution and 100 mg of CFA/GO/PANI + Cr(VI) at time intervals of 0−105 min at neutral pH as indicated in Figure 11A. Furthermore, studies were conducted on the effect of photolysis (blank experiment) on the degradation of BPA without CFA/GO/PANI + Cr(VI) at the same time interval as displayed in Figure 11B.

The BPA degradation with CFA/GO/PANI + Cr(VI) at a time of 105 min under visible light demonstrated a percentage degradation of 86% as presented in Figure 11C(a). It can be noticed from Figure 11C(b) that BPA photolysis under visible light irradiation is 12% at 105 min, indicating that photolysis under visible light alone within a short time has a negligible effect on BPA degradation. This result is in tandem with the reports of Garg et al. and Zhu.[56,57] These revealed that CFA/GO/PANI + Cr(VI) played a significant role in the effective degradation of BPA. CFA/GO/PANI + Cr(VI) was compared with other photocatalysts used in degradation of BPA and proved to be better because the degradation took lesser time and showed high efficiency as displayed in Table 5.

The degradation rate of BPA with CFA/GO/PANI + Cr(VI) was evaluated using the pseudo-first-order rate constant equation in eq 14 given below

$$\ln\left(\frac{C_t}{C_o}\right) = -Kt \tag{14}$$

where C_o and C_t are the initial concentration and concentration at time (t) of BPA under visible light, respectively. The rate constant was obtained from the slope of graph $\ln(C_o/C_t)$ against time. The estimated rate constant is 0.01356 min^{-1}. The result indicates that the photocatalytic degradation of BPA follows the pseudo-first-order model as presented in Figure 11D.

3.4. Mechanism of BPA Degradation Using CFA/GO/PANI + Cr(VI). Scheme 3 presents the proposed mechanism for BPA degradation using CFA/GO/PANI + Cr(VI) under visible

https://doi.org/10.1021/acsomega.2c05352
ACS Omega 2023, 8, 17523−17537

Scheme 2. Mechanism of Cr(VI) Ions Adsorption onto the CFA/GO/PANI Nanocomposite

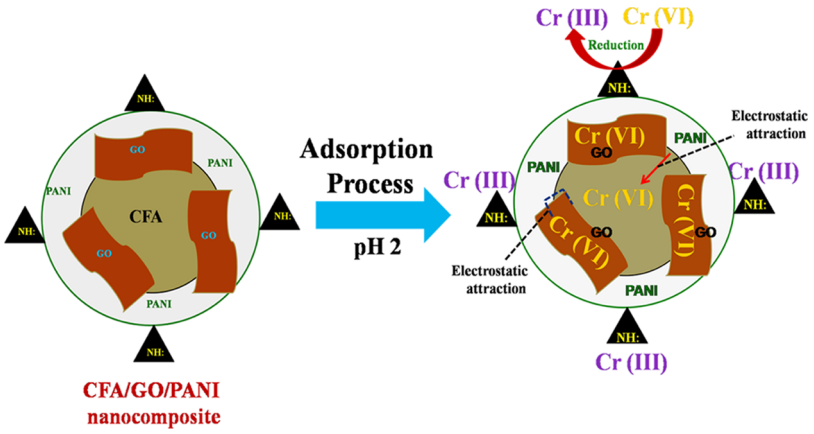

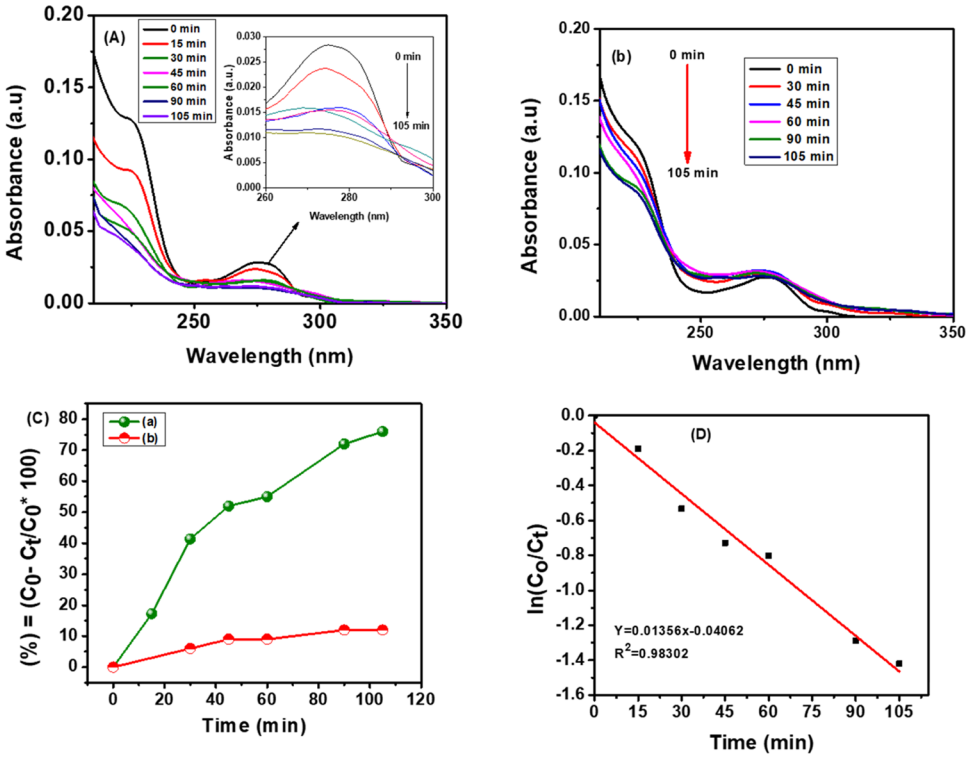

Figure 11. UV−vis spectra for BPA degradation with (A) CFA/GO/PANI + Cr(VI) and (B) photolysis and (C) BPA percentage degradation with (a) CFA/GO/PANI + Cr(VI) and (b) photolysis and (D) rate constant of CFA/GO/PANI + Cr(VI).

Table 5. BPA Photodegradation Using CFA/GO/PANI + Cr(VI) Compared with That with Other Catalysts

s.no	catalyst	degradation (%)	time (min)	references
1	Ag@TiO_2-PANI	99.7	120	7
2	N-codoped TiO_2	98	140	56
3	PW_{12}/TiO_2	77	720	58
4	rGO/Si/Zr	87	90	59
5	**CFA/GO/PANI + Cr(VI)**	**86**	**105**	**this study**

light. BPA was first adsorbed onto CFA/GO/PANI + Cr(VI) and later degraded by highly reactive radicals such as OH, O_2^-, and h^+ upon exposure to visible light due to the synergistic interaction between CFA, GO, PANI, and Cr(VI). PANI being a good conducting polymer and Cr(VI) with its photochemical effect both acted as antennae.

4. CONCLUSIONS

The prepared CFA/GO/PANI nanocomposite demonstrated outstanding results for Cr(VI) remediation from water and later showed the photocatalytic reuse possibility of the Cr(VI)-loaded spent adsorbent. The fabricated CFA/GO/PANI nanocomposite showed a high sorption capacity of 124.72 mg/g. The adsorption of Cr(VI) onto the CFA/GO/PANI nanocomposite was in agreement with pseudo-second-order kinetics and the Freundlich isotherm model. The adsorption mechanism revealed that the electrostatic interaction and reduction of Cr(VI) to Cr(III) occurred. Furthermore, the Cr(VI)-loaded spent adsorbent (CFA/GO/PANI + Cr(VI)) was effectively reused in photocatalytic degradation of BPA with a good degradation efficiency of 86%. The result for the percentage degradation can be attributed to the charge carrying and photoelectrochemical properties of Cr(VI). The reduction

https://doi.org/10.1021/acsomega.2c05352
ACS Omega 2023, 8, 17523−17537

Scheme 3. Photocatalytic Degradation of BPA Mechanism Using CFA/GO/PANI + Cr(VI)

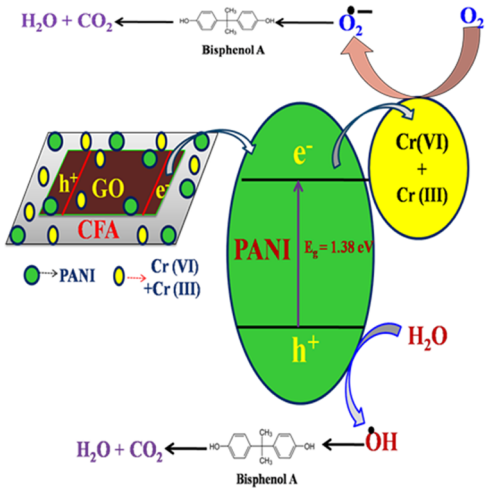

of Cr(VI) to Cr(III) from the XPS result is an indication that Cr(III) was also engaged in the photocatalysis.

AUTHOR INFORMATION

Corresponding Author

Kriveshini Pillay − *Department of Chemical Sciences, University of Johannesburg, Johannesburg 2028, South Africa;* orcid.org/0000-0002-2134-7666; Phone: +27 11 5596128; Email: kriveshinip@uj.ac.za; Fax: +27 11 5596425

Authors

Emmanuel Christopher Umejuru − *Department of Chemical Sciences, University of Johannesburg, Johannesburg 2028, South Africa*

Eswaran Prabakaran − *Department of Chemical Sciences, University of Johannesburg, Johannesburg 2028, South Africa*

Complete contact information is available at: https://pubs.acs.org/10.1021/acsomega.2c05352

Notes

The authors declare no competing financial interest.

ACKNOWLEDGMENTS

The authors would like to sincerely thank the National Research Foundation (NRF) for funding the research. The authors also sincerely thank Profs. Emanuela Carleschi and Bryan Doyle from the Department of Physics, University of Johannesburg, for performing the XPS analysis.

REFERENCES

(1) Chigondo, M.; Paumo, H. K.; Bhaumik, M.; Pillay, K.; Maity, A. Magnetic Arginine-Functionalized Polypyrrole with Improved and Selective Chromium(VI) Ions Removal from Water. *J. Mol. Liq.* **2019**, *275*, 778−791.

(2) Guidelines for Drinking-water Quality—World Health Organization, WHO—Google Books. https://books.google.co.za/books?hl=en&lr=&id=SJ76COTm-nQC&oi=fnd&pg=PR15&dq=F.+Edition,+Guidelines+for+drinking-water+quality,+WHO+Chron.,+2011,+38+104-108.&ots=V9uWpgVdXd&sig=etTDDUl97Wxt4JXa1q6Co5yMZVA&redir_esc=y#v=onepage&q&f=false (accessed Sep 3, 2022).

(3) Loock, M. M.; Beukes, J. P.; van Zyl, P. G. A Survey of Cr(VI) Contamination of Surface Water in the Proximity of Ferrochromium Smelters in South Africa. *Water SA* **2014**, *40*, 709−716.

(4) Mikhaylov, V. I.; Krivoshapkina, E. F.; Trigub, A. L.; Stalugin, V. V.; Krivoshapkin, P. V. Detection and Adsorption of Cr(VI) Ions by Mesoporous Fe-Alumina Films. *ACS Sustainable Chem. Eng.* **2018**, *6*, 9283−9292.

(5) Zhitkovich, A. Chromium in Drinking Water: Sources, Metabolism, and Cancer Risks. *Chem. Res. Toxicol.* **2011**, *24*, 1617−1629.

(6) Liu, Z.; Xu, Z.; Xu, L.; Buyong, F.; Chay, T. C.; Li, Z.; Cai, Y.; Hu, B.; Zhu, Y.; Wang, X. Modified Biochar: Synthesis and Mechanism for Removal of Environmental Heavy Metals. *Carbon Res.* **2022**, *1*, 1−21.

(7) Sambaza, S.; Maity, A.; Pillay, K. Enhanced Degradation of BPA in Water by PANI Supported Ag/TiO 2 Nanocomposite under UV and Visible Light. *J. Environ. Chem. Eng.* **2019**, *7*, No. 102880.

(8) Cui, Y.-W.; Li, J.; Du, Z.-F.; Peng, Y.-Z. Cr(VI) Adsorption on Red Mud Modified by Lanthanum: Performance, Kinetics and Mechanisms. *PLoS One* **2016**, No. e0161780.

(9) Amalraj, A.; Selvi, M. K.; Rajeswari, A.; Christy, E. J. S.; Pius, A. Efficient Removal of Toxic Hexavalent Chromium from Aqueous Solution Using Threonine Doped Polypyrrole Nanocomposite. *J. Water Process Eng.* **2016**, *13*, 88−99.

(10) Dash, S.; Chaudhuri, H.; Gupta, R.; Nair, U. G.; Sarkar, A. Fabrication and Application of Low-Cost Thiol Functionalized Coal Fly Ash for Selective Adsorption of Heavy Toxic Metal Ions from Water. *Ind. Eng. Chem. Res.* **2017**, *56*, 1461−1470.

(11) Feng, Z. Q.; Yuan, X.; Wang, T. Porous Polyacrylonitrile/Graphene Oxide Nanofibers Designed for High Efficient Adsorption of Chromium Ions (VI) in Aqueous Solution. *Chem. Eng. J.* **2020**, *392*, No. 123730.

(12) Sahoo, S. K.; Hota, G.; Amine-Functionalized, G. O. Decorated with ZnO-ZnFe2O4 Nanomaterials for Remediation of Cr(VI) from Water. *ACS Appl. Nano Mater.* **2019**, *2*, 983−996.

(13) Li, N.; Yue, Q.; Gao, B.; Xu, X.; Kan, Y.; Zhao, P. Magnetic Graphene Oxide Functionalized by Poly Dimethyl Diallyl Ammonium Chloride for Efficient Removal of Cr(VI). *J. Taiwan Inst. Chem. Eng.* **2018**, *91*, 499−506.

(14) Mansour, M. S.; Ossman, M. E.; Farag, H. A. Removal of Cd (II) Ion from Waste Water by Adsorption onto Polyaniline Coated on Sawdust. *Desalination* **2011**, *272*, 301−305.

(15) Eskandari, E.; Kosari, M.; Davood Abadi Farahani, M. H.; Khiavi, N. D.; Saeedikhani, M.; Katal, R.; Zarinejad, M. A Review on Polyaniline-Based Materials Applications in Heavy Metals Removal and Catalytic Processes. *Sep. Purif. Technol.* **2020**, *231*, No. 115901.

(16) Zhu, D.; Zhou, Q. Action and Mechanism of Semiconductor Photocatalysis on Degradation of Organic Pollutants in Water Treatment: A Review. *Environ. Nanotechnol., Monit. Manage.* **2019**, *12*, No. 100255.

(17) Lu, Y.; Cai, Y.; Zhang, S.; Zhuang, L.; Hu, B.; Wang, S.; Chen, J.; Wang, X. Application of Biochar-Based Photocatalysts for Adsorption -(Photo) Degradation/Reduction of Environmental Contaminants: Mechanism, Challenges and Perspective. *Biochar* **2022**, *4*, No. 13057.

(18) Hasija, V.; Raizada, P.; Sudhaik, A.; Sharma, K.; Kumar, A.; Singh, P.; Jonnalagadda, S. B.; Thakur, V. K. Recent Advances in Noble Metal Free Doped Graphitic Carbon Nitride Based Nanohybrids for Photocatalysis of Organic Contaminants in Water: A Review. *Appl. Mater. Today* **2019**, *15*, 494−524.

(19) Andronic, L.; Enesca, A.; Vladuta, C.; Duta, A. Photocatalytic Activity of Cadmium Doped TiO2 Films for Photocatalytic Degradation of Dyes. *Chem. Eng. J.* **2009**, *152*, 64−71.

(20) Umejuru, E. C.; Prabakaran, E.; Pillay, K. Coal Fly Ash Coated with Carbon Hybrid Nanocomposite for Remediation of Cadmium (II) and Photocatalytic Application of the Spent Adsorbent for Reuse. *Results Mater.* **2020**, *7*, No. 100117.

(21) Ahmed, A. M.; Rabia, M.; Shaban, M. The Structure and Photoelectrochemical Activity of Cr-Doped PbS Thin Films Grown by Chemical Bath Deposition. *RSC Adv.* **2020**, *10*, 14458−14470.

(22) Wang, L.; Hu, D.; Kong, X.; Liu, J.; Li, X.; Zhou, K.; Zhao, H. Anionic Polypeptide Poly(γ-Glutamic Acid)-Functionalized Magnetic Fe3O4-GO-(o-MWCNTs) Hybrid Nanocomposite for High-efficiency Removal of Cd (II), Cu (II) and Ni (II) Heavy Metal Ions. *Chem. Eng. J.* **2018**, *346*, 38−49.
(23) Sanchís, J.; Milačič, R.; Zuliani, T.; Vidmar, J.; Abad, E.; Farré, M.; Barceló, D. Occurrence of C60 and Related Fullerenes in the Sava River under Different Hydrologic Conditions. *Sci. Total Environ.* **2018**, *643*, 1108−1116.
(24) Muniyalakshmi, M.; Sethuraman, K.; Silambarasan, D. Synthesis and Characterization of Graphene Oxide Nanosheets. *Mater. Today Proc.* **2020**, *21*, 408−410.
(25) Ballav, N.; Maity, A.; Mishra, S. B. High Efficient Removal of Chromium(VI) Using Glycine Doped Polypyrrole Adsorbent from Aqueous Solution. *Chem. Eng. J.* **2012**, *198*−*199*, 536−546.
(26) Parande, A. K.; Stalin, K.; Kumar Thangarajan, R.; Karthikeyan, M. S.; Mang, H. A. Utilization of Agroresidual Waste in Effective Blending in Portland Cement. *Int. Scholarly Res. Not.* **2011**, *2011*, 12.
(27) Rawat, K.; Yadav, A. K. Characterization of Coal and Fly Ash (Generated) at Coal Based Thermal Power Plant. *Mater. Today Proc.* **2020**, *26*, 1406−1411.
(28) Bokare, A.; Nordlund, D.; Melendrez, C.; Robinson, R.; Keles, O.; Wolcott, A.; Erogbogbo, F. Surface Functionality and Formation Mechanisms of Carbon and Graphene Quantum Dots. *Diam. Relat. Mater.* **2020**, *110*, No. 108101.
(29) Zhang, H.; Wang, X.; Li, N.; Xia, J.; Meng, Q.; Ding, J.; Lu, J. Synthesis and Characterization of TiO 2 /Graphene Oxide Nanocomposites for Photoreduction of Heavy Metal Ions in Reverse Osmosis Concentrate. *RSC Adv.* **2018**, *8*, 34241−34251.
(30) Wei, J.; Liang, B.; Cao, Q.; Mo, C.; Zheng, Y.; Ye, X. Vertically Aligned PANI Nanorod Arrays Grown on Graphene Oxide Nanosheets for a High-Performance NH 3 Gas Sensor. *RSC Adv.* **2017**, *7*, 33510−33520.
(31) Bachhav, S. G.; Patil, D. R. Synthesis and Characterization of Polyaniline-Multiwalled Carbon Nanotube Nanocomposites and Its Electrical Percolation Behavior. *Am. J. Mater. Sci.* **2015**, *5*, 90−95.
(32) Parveen, N.; Mahato, N.; Ansari, M. O.; Cho, M. H. Enhanced Electrochemical Behavior and Hydrophobicity of Crystalline Polyaniline@graphene Nanocomposite Synthesized at Elevated Temperature. *Composites, Part B* **2016**, *87*, 281−290.
(33) Wang, L.; Ye, Y.; Lu, X.; Wen, Z.; Li, Z.; Hou, H.; Song, Y. Hierarchical Nanocomposites of Polyaniline Nanowire Arrays on Reduced Graphene Oxide Sheets for Supercapacitors. *Sci. Rep.* **2013**, *3*, No. 3568.
(34) Wu, Z.; Chen, X.; Zhu, S.; Zhou, Z.; Yao, Y.; Quan, W.; Liu, B. Enhanced Sensitivity of Ammonia Sensor Using Graphene/Polyaniline Nanocomposite. *Sens. Actuators, B* **2013**, *178*, 485−493.
(35) Zheng, M.; Ahn, Y.; Yoon, Y.; Park, W. K.; Jung, Y.; Kwon, M.; Yang, W. S.; Kang, J. W. Removal of Cr(VI) from Aqueous Solution Using Magnetite/Non-Oxidative Graphene Composites: Synergetic Effect of Cr(VI) on Dyes Removal. *Sep. Sci. Technol.* **2016**, *51*, 2958−2969.
(36) Khan, R.; Khare, P.; Baruah, B. P.; Hazarika, A. K.; Chandra Dey, N. Spectroscopic, Kinetic Studies of Polyaniline-Flyash Composite. *Adv. Chem. Eng. Sci.* **2011**, *1*, 37−44.
(37) Zhang, H.; Tang, Y.; Cai, D.; Liu, X.; Wang, X.; Huang, Q.; Yu, Z. Hexavalent Chromium Removal from Aqueous Solution by Algal Bloom Residue Derived Activated Carbon: Equilibrium and Kinetic Studies. *J. Hazard. Mater.* **2010**, *181*, 801−808.
(38) Shyaa, A. A.; Hasan, O. A.; Abbas, A. M. Synthesis and Characterization of Polyaniline/Zeolite Nanocomposite for the Removal of Chromium(VI) from Aqueous Solution. *J. Saudi Chem. Soc.* **2015**, *19*, 101−107.
(39) Xu, G.; Wang, N.; Wei, J.; Lv, L.; Zhang, J.; Chen, Z.; Xu, Q. Preparation of Graphene Oxide/Polyaniline Nanocomposite with Assistance of Supercritical Carbon Dioxide for Supercapacitor Electrodes. *Ind. Eng. Chem. Res.* **2012**, *51*, 14390−14398.
(40) Khasim, S. Polyaniline-Graphene Nanoplatelet Composite Films with Improved Conductivity for High Performance X-Band Microwave Shielding Applications. *Results Phys.* **2019**, *12*, 1073−1081.
(41) Miao, J.; Li, H.; Qiu, H.; Wu, X.; Yang, J. Graphene/PANI Hybrid Film with Enhanced Thermal Conductivity by in Situ Polymerization. *Science* **2018**, *53*, 8855−8865.
(42) Zhang, W.; Lan, Y.; Ma, M.; Chai, S.; Zuo, Q.; et al. A Novel Chitosan—Vanadium-Titanium-Magnetite Composite as a Superior Adsorbent for Organic Dyes in Wastewater. *Environ. Int.* **2020**, *142*, No. 105798.
(43) Singh, S. K.; Verma, A. K.; Shukla, R. K. Synthesis and Optical Studies of Pure Polyaniline Film. *Int. J. Curr. Microbiol. Appl. Sci.* **2014**, *3*, 512−517.
(44) Ouyang, D.; Zhuo, Y.; Hu, L.; Zeng, Q.; Hu, Y.; He, Z. Minerals Research on the Adsorption Behavior of Heavy Metal Ions by Porous Material Prepared with Silicate Tailings. *Minerals* **2019**, *9*, No. 291.
(45) Lin, Y. J.; Chen, J. J.; Cao, W. Z.; Persson, K. M.; Ouyang, T.; Zhang, L.; Xie, X.; Liu, F.; Li, J.; Chang, C. T. Novel Materials for Cr(VI)Adsorption by Magnetic Titanium Nanotubes Coated Phosphorene. *J. Mol. Liq.* **2019**, *287*, No. 110826.
(46) Parashar, K.; Ballav, N.; Debnath, S.; Pillay, K.; Maity, A. Hydrous ZrO2 Decorated Polyaniline Nanofibres: Synthesis, Characterization and Application as an Efficient Adsorbent for Water Defluoridation. *J. Colloid Interface Sci.* **2017**, *508*, 342−358.
(47) Qiu, B.; Xu, C.; Sun, D.; Yi, H.; Guo, J.; Zhang, X.; Qu, H.; Guerrero, M.; Wang, X.; Noel, N.; Luo, Z.; Guo, Z.; Wei, S. Polyaniline Coated Ethyl Cellulose with Improved Hexavalent Chromium Removal. *ACS Sustainable Chem. Eng.* **2014**, *2*, 2070−2080.
(48) Rai, M. K.; Shahi, G.; Meena, V.; Meena, R.; Chakraborty, S.; Singh, R. S.; Rai, B. N. Removal of Hexavalent Chromium Cr (VI) Using Activated Carbon Prepared from Mango Kernel Activated with H3PO4. *Resour. Technol.* **2016**, *2*, S63−S70.
(49) Sathvika, T.; Raj, A.; Saraswathi, K.; Rajesh, V.; Rajesh, N. Confluence of Montmorillonite and Rhizobium towards the Adsorption of Chromium(VI) from Aqueous Medium. *RSC Adv.* **2019**, *9*, 28478−28489.
(50) Qiu, B.; Xu, C.; Sun, D.; Wang, Q.; Gu, H.; Zhang, X.; Weeks, B. L.; Hopper, J.; Ho, T. C.; Guo, Z.; Wei, S. Polyaniline Coating with Various Substrates for Hexavalent Chromium Removal. *Appl. Surf. Sci.* **2015**, *334*, 7−14.
(51) Kumar, R.; Ansari, M. O.; Barakat, M. A. DBSA Doped Polyaniline/Multi-Walled Carbon Nanotubes Composite for High Efficiency Removal of Cr(VI) from Aqueous Solution. *Chem. Eng. J.* **2013**, *228*, 748−755.
(52) Kera, N. H.; Bhaumik, M.; Pillay, K.; Ray, S. S.; Maity, A. Selective Removal of Toxic Cr(VI) from Aqueous Solution by Adsorption Combined with Reduction at a Magnetic Nanocomposite Surface. *J. Colloid Interface Sci.* **2017**, *503*, 214−228.
(53) Cheng, H.; Zhu, R.; Zhang, P.; Wu, D.; Tang, Q.; Duan, T.; Li, P. Enhanced Defluoridation Capacity From Aqueous Media via Hydroxyapatite Decorated With Carbon Nanotube. *Front. Chem.* **2018**, *1*, No. 104.
(54) Dong, L.; Liang, J.; Li, Y.; Hunang, S.; Wei, Y.; Bai, X.; Jin, Z.; Zhang, M.; Qu, J. Effect of Coexisting Ions on Cr(VI) Adsorption onto Surfactant Modified Auricularia Auricula Spent Substrate in Aqueous Solution. *Ecotoxicol. Environ. Saf.* **2018**, *166*, 390−400.
(55) Sahoo, J. K.; et al. Surface Functionalization of Graphene Oxide Using Amino Silane Magnetic Nanocomposite for Chromium (VI) Removal and Bacterial Treatment. *Nano Express* **2020**, No. 010062.
(56) Garg, A.; Singhania, T.; Singh, A.; Sharma, S.; Rani, S.; Neogy, A.; Ram Yadav, S.; Kumar sangal, V.; Garg, N. Photocatalytic Degradation of Bisphenol-A Using N, Co Codoped Tio 2 Catalyst under Solar Light. *Sci. Rep.* **2019**, *9*, No. 765.
(57) Zhu, Y.; Zhu, R.; Xi, Y.; Xu, T.; Yan, L.; Zhu, J.; Zhu, G.; He, H. Heterogeneous Photo-Fenton Degradation of Bisphenol A over Ag/AgCl/Ferrihydrite Catalysts under Visible Light. *Chem. Eng. J.* **2018**, *346*, 567−577.
(58) Lu, N.; Lu, Y.; Liu, F.; Zhao, K.; Yuan, X.; Zhao, Y.; Li, Y.; Qin, H.; Zhu, J. H3PW12O40/TiO2 Catalyst-Induced Photodegradation of

https://doi.org/10.1021/acsomega.2c05352
ACS Omega 2023, 8, 17523−17537

Bisphenol A (BPA): Kinetics, Toxicity and Degradation Pathways. *Chemosphere* **2013**, *91*, 1266−1272.
(59) Hassan, N. S.; Jalil, A. A.; Khusnun, N. F.; Ali, M. W.; Haron, S. Role of Reduced Graphene Oxide in Improving Interfacial Charge Transfer of Hybridized RGO/Silica/Zirconia for Enhanced Bisphenol A Photodegradation. *J. Alloys Compd.* **2019**, *789*, 221−230.

https://doi.org/10.1021/acsomega.2c05352
ACS Omega 2023, 8, 17523−17537